SIAM J. SCI. COMPUT.
Vol. 26, No. 1, pp. 240–258

THE REDUCED BASIS ELEMENT METHOD: APPLICATION TO A THERMAL FIN PROBLEM*

YVON MADAY† AND EINAR M. RØNQUIST‡

Abstract. The reduced basis element method is a new approach for the approximation of partial differential equations that takes its roots in the domain decomposition method and in the reduced basis discretization. The basic idea is to decompose the domain of computation into a series of subdomains (the elements) that are similar to a few reference domains. These reference domains are actually "filled" with reduced basis functional spaces that are mapped to each subdomain together with the geometry. The discrete approximation space is then composed of functions with the property that a function restricted to a subdomain belongs to the mapped reduced spaces. Finally, a mortar-type method is applied to glue the various local functions. In this paper we focus on the definition of the reference shapes, and together with theoretical and numerical justifications of the method, we provide a posteriori error analysis tools that allow us to certify the computational results.

Key words. reduced basis, reduced order model, domain decomposition, mortar method, output bounds, a posteriori error estimators

AMS subject classifications. 65C20, 93A30, 65N30, 65N35, 65N15, 80A20

DOI. 10.1137/S1064827502419932

1. Introduction.

A *reduced basis element* method was introduced in [10] in the context of solving the Laplace problem on a deformed geometry. The basic idea consists in combining domain decomposition techniques with reduced basis approximations.

On the one hand, domain decomposition approaches are classically of interest for at least two reasons: the first one is to enable the use of parallel architectures in order to speed up the solution time compared to a global approach; the second reason is to generalize a discretization method that is originally designed over a simple geometry, like the extension of the spectral method to the spectral element discretization. This latter aspect is a first basic ingredient of the reduced basis element method.

On the other hand, reduced basis methods have been introduced in [11] and [6] to obtain a good approximation by solving very small discrete systems. The idea is that, in the frame of problems that appear as partial differential equations depending on some (family of) parameters, the dependency of the solution on the parameters is most often regular so that the generic solution (as a function of the parameters) can be well approximated by some linear combination of the solutions precomputed for certain instances of the parameters. This is the second basic ingredient of the reduced basis element method.

Our method takes into account these features in a new point of view as the parameters that are referred to represent the shape of the domain. In this sense, the method represents a generalization as, to our knowledge, previous choices of the parameters always belong to a subset of $\mathbb{R}^p$, $p \in \mathbb{N}$; here, the shapes live in some

*Received by the editors December 18, 2002; accepted for publication (in revised form) December 19, 2003; published electronically November 9, 2004.
http://www.siam.org/journals/sisc/26-1/41993.html
†Laboratoire Jacques-Louis Lions, Université Pierre et Marie Curie, 75252 Paris, Cedex 05, France (maday@ann.jussieu.fr).
‡Department of Mathematical Sciences, NTNU, N-7491, Trondheim, Norway (ronquist@math.ntnu.no).

infinite-dimensional space.

The introduction to our method is as follows. The computational domain of interest is first decomposed into several subdomains, each of them being the deformation of one or a few generic, *reference* building blocks. As a precomputation, the Laplace problem is solved over various deformations of each reference building block and stored, after mapping, on the associated reference building block; here, the spectral element method is used to precompute these solutions, but other standard discretizations can be used as well. The solution corresponding to an unknown, deformed geometry is then represented as a linear combination of the precomputed solutions mapped from the reference building block onto each particular subdomain of interest, and the matching between the different subdomains is ensured through the use of Lagrange multipliers. Very rapid convergence can be observed.

In this paper we extend the generality of the computation by introducing more complex reference building blocks. In addition, we introduce an a posteriori error estimator that can be advocated in order to certify the approximations of some output. These latter results extend to our context the general literature on *bounds on outputs* for which we refer to, e.g., [7, 12, 13].

2. Definition of the thermal fin problem.

2.1. Strong formulation. The particular problem we study is the heat conduction in a thermal fin. This problem has previously been used as a test problem in the context of developing and computing output bounds for partial differential equations for other types of reduced basis approximations; see [7].

A typical three-stage thermal fin is depicted and described in Figure 1. A constant heat flux, q, is prescribed at the root of the fin and may represent the heat generated from an electronic device, say. The purpose of the fin is to effectively remove this heat. In general, we may have K such stages; in what follows we shall introduce our methodology on this particular geometry ($K = 3$) for the sake of clarity.

We assume that the fin can be assembled from a few different types of material,

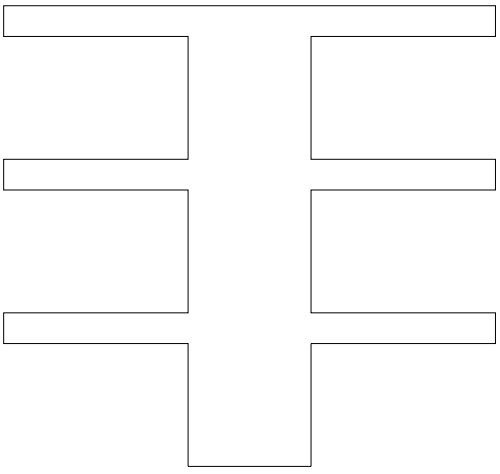

FIG. 1. *The geometry of the thermal fin problem. The fin consists of three stages, with the root of the fin at the bottom.*

each with a constant thermal conductivity. In general, Ω_i^m will denote the part of the fin which is made from the same material m_i and which has an associated thermal conductivity $k_i > 0$. In particular, we denote the central piece of the fin as Ω_0^m and the corresponding conductivity as $k_0 > 0$. The two subfins (left and right) associated with stage i are denoted as Ω_i^m and are assumed to be made from the same material with conductivity k_i; however, the conductivities may be different in the different stages $i = 1, 2, 3$.

We assume no heat generation within the thermal fin itself. The heat flux entering the fin at the fin root, Γ_{root}, will leave through the remaining surface of the fin. At steady state, the heat flux entering at the fin root must equal the total heat loss.

In order to model the heat loss from the fin surface, we prescribe the Robin boundary conditions

$$-k_i \frac{\partial u}{\partial n} = \text{Bi}\ u \quad \text{on} \quad \Gamma_i^m, \ \ i = 0, 1, 2, 3. \tag{2.1}$$

Here, Γ_i^m denotes the external fin surface associated with Ω_i^m, Bi is the Biot number ($\text{Bi} > 0$), and u denotes the temperature. The Robin boundary condition models heat loss due to convection, and a high Biot number means a more effective heat removal for a given (normalized) surrounding temperature equal to zero.

The governing equation for the temperature u in the fin is the Laplace equation within each subregion Ω_i^m, $i = 0, 1, 2, 3$. More precisely,

$$k_i \nabla^2 u = 0 \quad \text{in} \quad \Omega_i^m, \ \ i = 0, 1, 2, 3. \tag{2.2}$$

On the internal interface $\Gamma_{0,i}^m$ between the central piece Ω_0^m and the subfins Ω_i^m, $i = 1, 2, 3$, continuity of the temperature and the heat flux is required.

2.2. Weak formulation. The weak formulation of the thermal fin problem can be stated as follows: Find $u \in H^1(\Omega)$ such that

$$a(u, v) = f(v) \qquad \forall\, v \in H^1(\Omega), \tag{2.3}$$

where

$$a(u, v) = \sum_{i=0}^{3} k_i \int_{\Omega_i^m} \nabla u \cdot \nabla v \ dA \ + \ \text{Bi} \sum_{i=0}^{3} \int_{\Gamma_i^m} u\, v \ dS, \tag{2.4}$$

$$f(v) = \int_{\Gamma_{\text{root}}} q\, v \ dS. \tag{2.5}$$

We note that $a(\cdot, \cdot)$ is a symmetric, positive definite bilinear form, and $f(\cdot)$ is a linear form. It is standard to show that this problem has a unique solution u.

2.3. Spectral element solution. One straightforward way to solve the thermal fin problem (2.3)–(2.5) is to apply a standard Galerkin-type method. For example, Figure 2 depicts a spectral element discretization comprising $\mathcal{K} = 12$ spectral elements or subdomains Ω_k^e, $k = 1, \ldots, \mathcal{K}$; the center piece of the fin Ω_0^m consists of six spectral elements (two elements per stage of the fin), while each subfin consists of a single spectral element. The solution within each spectral element is approximated as a polynomial of degree $\mathcal{N} = 20$ in each spatial direction.

In terms of domain decomposition, we remark that

$$\overline{\Omega} = \cup_{i=0}^{K} \overline{\Omega}_i^m = \cup_{k=1}^{\mathcal{K}} \overline{\Omega}_k^e, \tag{2.6}$$

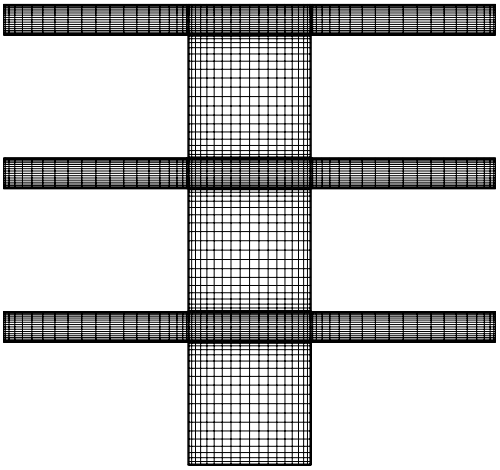

FIG. 2. *Spectral element grid associated with the thermal fin problem. The three-stage fin is decomposed into* $\mathcal{K} = 12$ *elements, each of order* $\mathcal{N} = 20$.

where superscript m is associated with a decomposition into different *materials*, while superscript e is associated with a decomposition into different *elements*.

Next, we define the finite-dimensional subspace $\mathcal{X}^{\mathcal{N}}$ of $H^1(\Omega)$ consisting of all functions which are polynomials of degree $\mathcal{N}$ over each spectral element Ω_k^e, $k = 1, \ldots, \mathcal{K}$, and which are continuous across internal boundaries between adjacent elements. Mathematically, we can express $\mathcal{X}^{\mathcal{N}}$ as

$$\mathcal{X}^{\mathcal{N}} = \{\, v \in H^1(\Omega),\ \ v_{|\Omega_k^e} \in \mathbb{P}_{\mathcal{N}}(\Omega_k^e),\, k = 1, \ldots, \mathcal{K}\,\}. \tag{2.7}$$

The spectral element formulation for the thermal fin problem can then be stated as follows: Find $u^{\mathcal{N}} \in \mathcal{X}^{\mathcal{N}}$ such that

$$a^{\mathcal{N}}(u^{\mathcal{N}}, v) = f^{\mathcal{N}}(v) \qquad \forall\, v \in \mathcal{X}^{\mathcal{N}}, \tag{2.8}$$

where $a^{\mathcal{N}}$ and $f^{\mathcal{N}}$ in (2.8) denote evaluation of the integrals appearing in the bilinear and linear forms in (2.4)–(2.5) by Gauss–Lobatto quadrature; see [8]. The method is thus a conforming method. It is well known that the following error estimate holds: for any s such that $u_{|\Omega_k^e} \in H^s(\Omega_k^e)$,

$$\|u - u^{\mathcal{N}}\|_{H^1(\Omega)} \ \le\ c\, N^{1-s} \sum_{k=1}^{\mathcal{K}} \|u_{|\Omega_k^e}\|_{H^s(\Omega_k^e)}\,.$$

For the discretization shown in Figure 2, the total number of degrees-of-freedom is approximately $\mathcal{K} \times \mathcal{N}^2 = 4800$. Figure 3 shows the corresponding spectral element solution $u^{\mathcal{N}}$ in terms of temperature contours. The choice of parameters for this particular thermal fin problem is $k_0 = 1.0$, $k_1 = 0.4$, $k_2 = 0.6$, $k_3 = 0.8$, $q = 1$, and $\mathrm{Bi} = 0.1$. This computation will serve as *the* reference in what follows as spectral element approximations with degree 20 can be assumed to be largely accurate enough for most applications.

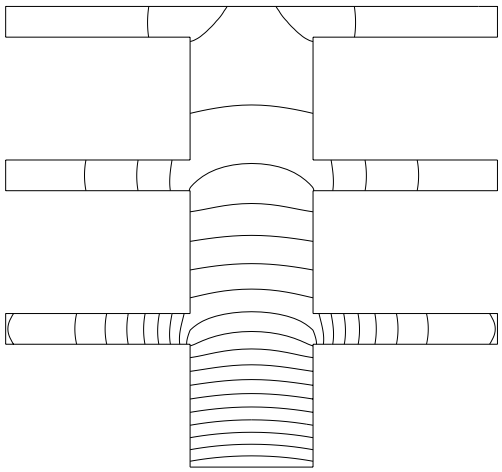

FIG. 3. *Temperature contours corresponding to the spectral element solution. Note that this steady state solution is symmetric.*

3. Reduced basis element method: Basic features. We observe that the global solution to the thermal fin problem is characterized by a certain amount of "repetitiveness" of the local solution behavior. The temperature drop through the central piece of the fin, as well as through the individual subfins, exhibits some degree of similarity: each individual spectral element of the fin is made of a material with a constant thermal conductivity; the governing equation within each individual spectral element is the Laplace equation; the "boundary conditions" along the surface of each individual element consist of one side with an incoming thermal heat flux, while the heat is leaving through the remaining sides.

The idea behind using the reduced basis element method for this problem is threefold: (i) to decompose the geometry Ω into elementary bricks that resemble a fixed reference shape $\hat{\Omega}$; (ii) to express the approximate numerical solution within each particular brick as a linear combination of precomputed solutions for similar parts; (iii) to glue together the solutions on the individual parts by using Lagrange multipliers. Let us now proceed with more details.

3.1. A first choice of reduced basis elements. The natural choice of elementary bricks consists of a decomposition into rectangles Ω_k. The objective is to construct a (small) set of basis functions which can be used to approximate the solution over a reference domain (here, $\hat{\Omega} = (-1, 1)^2$) with a constant thermal conductivity. The idea is then to reuse this basis set over each part of the thermal fin (here, in each spectral element), and to glue together the individual solutions to form a global solution for the entire fin.

In order to precompute the basis functions, we compute the temperature solution corresponding to one or more smaller fin problems, in particular, fin problems with only a single stage. Specifically, we compute the spectral element solution in a geometry depicted in Figure 4. The domain is discretized into four rectangular spectral elements. The central part of the fin is comprised of the two elements in the middle, and the associated thermal conductivity is k_0 in both elements. The subfin to the left has a thermal conductivity k_{left}, while the subfin to the right has a thermal

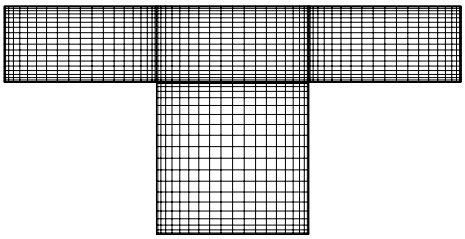

FIG. 4. *The geometry of the (small) thermal fin problem used in order to construct a first choice of reduced basis functions.*

TABLE 1
Choice of parameters.

Snapshot	k_0	k_{left}	k_{right}	Bi
1	1.0	0.4	0.8	0.1
2	1.0	0.4	0.8	0.2
3	1.0	0.2	1.0	0.1

conductivity k_{right}. Note that the left and right subfins are shorter and thicker than the subfins on the three-stage thermal fin we are actually interested in. Also note that, while the real subfins have the same conductivity at each stage, the subfins in the sample problems are different ($k_{\text{left}} \neq k_{\text{right}}$). The boundary conditions are similar to the three-stage fin: a specified heat flux q at the root of the fin (the bottom surface) and Robin boundary conditions along the remaining external surface.

We solve three instantiations (or snapshots) of this smaller fin problem. The associated choice of parameters is shown in Table 1. Note that all the precomputed solutions are asymmetric, while the solution for the three-stage fin is symmetric with respect to the vertical center line; see Figure 3.

The reduced basis is now constructed as follows: for each snapshot, the spectral element solution restricted to each of the four spectral elements (or subdomains) is defined as an element in the reduced basis. In this way, a single snapshot generates four basis functions. These basis functions are represented on the reference domain $\hat{\Omega}$ ($\equiv (-1,1)^2$) and will be denoted as w_i, $i = 1, 2, 3, 4$. All the basis functions w_i are oriented in such a way that the heat flux into the reference domain corresponds to the same surface for all the basis functions. For example, if (ξ, η) represents a point in the reference domain, the surface $\eta = -1$ may correspond to the surface where the normal derivative of the solution is negative (i.e., the heat flux is directed into the domain). Note that here we take into account some natural facts about the physics of the phenomenon. This allows us to further reduce the size of the reduced basis set.

In order to minimize potential directional effects, we enrich the basis by reflecting each basis function w_i around the line $\xi = 0$ on the reference domain; this approach

will thus generate a total of $4 \times 2 = 8$ individual basis functions $\{w_i\}_{i=1}^{8}$ for each snapshot. With two snapshots, we generate 16 basis functions, and with three snapshots, we generate 24 basis functions. This compares to the original $20^2 = 400$ basis functions used within a single element. In other words, we approximate the temperature within a single element using very few basis functions. However, we repeat that each of the reduced basis functions is represented using the "conventional" spectral element basis. The key point is that the reduced basis is more "tailored" toward the particular type of application that we are interested in. The number of stages in the fin and the types of material associated with the individual parts may vary from case to case, but the solution within a particular part can hopefully be described by a few representative basis functions.

At this point, one additional comment is in order. The previous discussion has tacitly assumed that all the precomputed basis functions are linearly independent (as elements of $L^2(\hat{\Omega})$). The asymmetric sample solutions shown earlier will ensure that this is not obviously false. However, the basis functions may be close to being linearly dependent, leading to lack of stability with respect to round-off errors. This is particularly noticeable if we include three snapshots instead of two. In order to make sure that the basis functions are, in fact, far from being linearly dependent, we perform a modified Gram–Schmidt orthogonalization of all the basis functions with respect to the inner product associated with the usual energy norm.

3.2. Reduced basis solution with two snapshots. We consider first a reduced basis constructed from snapshots 1 and 2. Armed with a precomputed set comprising $M = 16$ basis functions $\{w_i\}_{i=1}^{16}$, which are all represented on the reference domain $\hat{\Omega}$, we are in a position to define a reduced basis element formulation of the three-stage fin problem. The 16 reduced basis functions are mapped from the reference domain $\hat{\Omega}$ to each of the $\mathcal{K} = 12$ spectral elements Ω_k^e, $k = 1, \ldots, \mathcal{K}$, in the fin; we denote the corresponding mappings Φ_k, $k = 1, \ldots, \mathcal{K}$. Note that these mappings should be chosen so that the image of the surface $\eta = -1$ through Φ_k corresponds to the surface where the energy enters the subdomain $\Phi_k(\hat{\Omega})$. Note also that all the mappings are chosen with positive Jacobian determinant.

Next, we introduce the (first) finite-dimensional space

$$Y_M^1 = \{\, v \in L^2(\Omega), \quad v_{|\Omega_k} \circ \Phi_k \in \mathrm{Span}\{w_i\}_{i=1}^{M} \,\}. \tag{3.1}$$

In order to propose an admissible discrete space for $H^1(\Omega)$, we have to glue together the values of elements of Y_M^1 through each interface $\Gamma_{k,\ell}^e$ between two adjacent spectral elements Ω_k^e and Ω_ℓ^e. As is often the case, the exact coincidence of the traces of the discrete functions is generally too stringent; thus, the gluing process is done in a dual way through Lagrange multipliers. We denote by $W_{k,\ell}$ a set of functions over each interface $\Gamma_{k,\ell}^e$, and we define

$$X_M^1 = \left\{ v \in Y_M^1, \quad \forall k, \ell, \quad \forall \psi \in W_{k,\ell}, \int_{\Gamma_{k,\ell}^e} (v^+ - v^-)\psi \; ds \; = \; 0 \right\}, \tag{3.2}$$

where, for a given v in Y_M^1 and any interface $\Gamma_{k,\ell}^e$, $v_{\Gamma_{k,\ell}^e}^+ (= v^+)$ and $v_{\Gamma_{k,\ell}^e}^- (= v^-)$ stand for the two values that v takes on each side of $\Gamma_{k,\ell}^e$. For later use, we denote by $[v]$ the jump $[v] = v^+ - v^-$.

Of course, the approximation space is generally not a subspace of $H^1(\Omega)$ and the method is nonconforming. The definition of the Lagrange multiplier space $W_{k,\ell}$ has to

be done in a proper way and can also be defined through a mapping from a reference space of test functions over the reference interval $]-1,1[$.

The discrete problem based on a reduced basis element method can now be defined as follows: Find $u_M^1 \in X_M^1$ such that

$$a^{\mathcal{N}}(u_M^1, v) = f^{\mathcal{N}}(v) \qquad \forall\, v \in X_M^1, \tag{3.3}$$

where $a^{\mathcal{N}}$ and $f^{\mathcal{N}}$ denote the same bilinear and linear forms as in (2.8). Again, it is an easy matter to check that this problem is well posed.

We thus see that the best linear combination of the precomputed basis functions $\{w_i\}$, mapped to each spectral element, is found via a Galerkin procedure. For the spectral element including the root of the fin, the prescribed flux boundary condition is satisfied in a weak sense through the linear form $f(\cdot)$. Along the remaining boundary, the Robin boundary conditions are taken care of through the definition of the bilinear form $a(\cdot,\cdot)$. Finally, along all the internal boundaries between adjacent spectral elements, the jump in the solution is assumed to be orthogonal to all elements belonging to a predefined Lagrange multiplier space in the spirit of the mortar element method [5, 1].

The standard tool for analyzing such a nonconforming discretization method is the Berger–Scott–Strang lemma [2] that with our notation yields

$$\|u - u_M^1\|_* \le c \left(\inf_{v_M \in X_M^1} \|u - v_M\|_* + \sup_{w_M \in X_M^1} \frac{\sum_{k,\ell} \int_{\Gamma_{k,\ell}^e} \frac{\partial u}{\partial n} [w_M]}{\|w_M\|_*} \right), \tag{3.4}$$

where the norm $\|.\|_*$ (resp., the seminorm $|.|_*$) is known as the "broken norm" (resp., the "broken seminorm") and is defined by

$$\forall v \in Y_M^1, \quad \|v\|_*^2 = \sum_{k=1}^{\mathcal{K}} \|v_{|\Omega_k^e}\|_{H^1(\Omega_k^e)}^2, \quad \left(\text{resp., } |v|_*^2 = \sum_{k=1}^{\mathcal{K}} |v_{|\Omega_k^e}|_{H^1(\Omega_k^e)}^2 \right).$$

The first term in the error bound (3.4) is known as the best fit error contribution, while the second term is known as the consistency error contribution and is the consequence of the nonconformity of the method. The objective is to have these two contributions small and of the same order.

In summary, with $M = 16$ basis functions $\{w_i\}$ and a Lagrange multiplier space $W_{k,\ell} = \mathbb{P}_2(\Gamma_{k,\ell}^e)$ over each $\Gamma_{k,\ell}^e$, this procedure gives rise to a system of algebraic equations of size 225; the structure of this system is depicted in Figure 5. The system is solved using standard Gaussian elimination. The maximum pointwise error is 0.038, approximately 2%.

In the example just mentioned, we defined our Lagrange multiplier space as $W_{k,\ell} = \mathbb{P}_2(\Gamma_{k,\ell}^e)$, i.e., consisting of low order polynomials of maximum degree equal to 2. In the table below, we compare the maximum pointwise error for the same case, but with $W_{k,\ell} = \mathbb{P}_n(\Gamma_{k,\ell}^e)$, and with $n = 1, 2, \ldots, 10$. We notice that a fairly broad minimum is reached for values of n in the range 2–5. As expected, increasing n too much gives too stringent continuity requirements, and a resulting error increase is observed.

It could also be interesting to define the Lagrange multiplier space in a different fashion, taking more into account the singular behavior near the sharp corners of the fin. To this end, we consider the first snapshot in Table 1 which we denote as u_1.

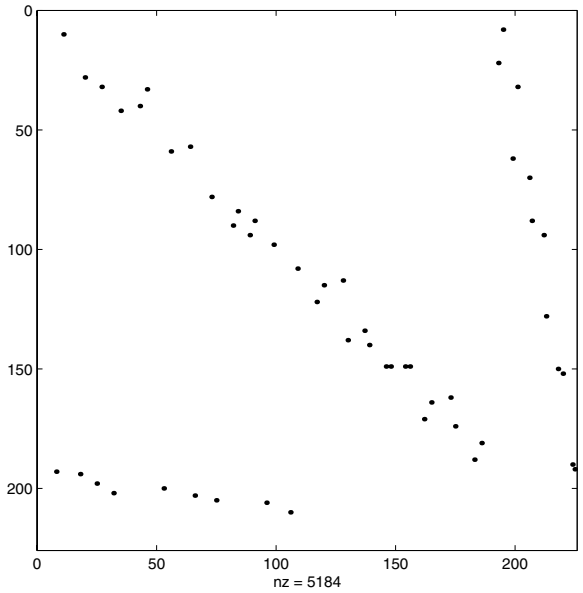

FIG. 5. *The matrix structure associated with computing the reduced basis coefficients for the three-stage thermal fin problem.*

TABLE 2

n	1	2	3	5	7	9
L^∞-error	0.057	0.038	0.034	0.034	0.042	0.082

In particular, we consider the normal derivative of u_1 along the two internal vertical interfaces which we simply denote as Γ_{left} and Γ_{right}. We then define the Lagrange multiplier space as

$$\forall k, \ell, \qquad W_{k,\ell} = \text{span}\left\{ \frac{\partial u_1}{\partial x}_{|\Gamma_{\text{left}}}, \frac{\partial u_1}{\partial x}_{|\Gamma_{\text{right}}}, \text{ reflections} \right\}. \tag{3.5}$$

Here, "reflections" means that we also include the reflected (or symmetric) versions of the two precomputed traces in $W_{k,\ell}$. Note that $W_{k,\ell}$ now consists of functions which are polynomials of degree $\mathcal{N} = 20$; i.e., the functions are of high polynomial degree. However, the dimension of $W_{k,\ell}$ defined in (3.5) is equal to 4, which can be compared with the dimension of $W_{k,\ell}$ when we instead use low order polynomials with $n = 3$. As in the first test, we use 16 basis functions inside each element. The maximum pointwise error is now 0.028, which should be compared to the earlier value of 0.034 reported in Table 2.

Note that we could also define the Lagrange multiplier space in many other ways, for example, by using other snapshots than the first one, or including the y-derivative of the sample solutions along internal horizontal interfaces. We have also experimented with this; however, the result shown in Table 2 seems to be typical. This may indicate that the governing error in (3.4) is then the best fit error and not the consistency error any more. This is confirmed by other numerical experiments that we have run that consist of defining the Lagrange multiplier space based on traces of the normal

derivative of the reference solution $u^{\mathcal{N}}$ so that the consistency error is zero; even then, the error is not improved.

3.3. Reduced basis solution with three snapshots. As a final test case, we now enrich the basis by also including snapshot number 3; see Table 2. The total number of basis functions within each element is therefore $M = 24$ (including reflections). In reference to the end of the previous subsection, this will allow us to diminish the best fit error. As mentioned earlier, we perform a modified Gram–Schmidt orthogonalization of the precomputed basis functions in order to improve the stability properties of the resulting system of algebraic equations; without orthogonalization, we experienced stability problems. The maximum pointwise error with $W_{k,\ell} = \mathbb{P}_3(\Gamma^e_{k,\ell})$ is now 0.016, which means a reduction by a factor of 2 compared to the case with two snapshots (see Table 2).

3.4. Some comments and comparison with standard approximations. At this point, a natural question to ask is how the accuracy and cost of using a reduced basis element method compares with a standard approximation consisting of simply using a low order polynomial approximation inside each spectral element. We will comment on this question now.

Consider the case where we use a standard, conforming spectral element discretization for the three-stage fin problem. As before, each stage consists of four spectral elements; however, the polynomial degree is now $\mathcal{N} = 4$. Taking into account the boundary conditions for this problem, the total number of unknowns for this discretization is 245. The associated maximum pointwise error is 0.026, which is roughly at the same level of error as the reduced basis approach described earlier for a comparable number of degrees-of-freedom.

At this point, it may be natural to conclude that it is better to simply use a coarse discretization instead of a reduced basis approach. A standard approximation is certainly simpler to use. However, it is also remarkable that the reduced basis element method is, as exemplified in this simple version, as accurate as the spectral element method that is recognized for its infinite order accuracy and its ability to approximate even corner singularities well; see [4]. It is furthermore interesting to reflect on whether the reduced basis approach has been used in the most appropriate way for this problem, or whether there is a more optimal way of constructing reduced basis functions. This issue will be topic of the next section.

4. Reduced basis element method: Efficiency and reliability. In this section, we want to address a more ad hoc reduced basis element method, as the building block will be more tuned to the particular geometry we have at hand. We shall now also consider more general fins in the sense that they may have various number of stages and that each stage may be different. Finally, we will discuss a posteriori error estimation.

4.1. A second choice of reduced basis elements. Let Ω be the geometry of the fin of interest. We assume it is composed of K stages, i.e.,

$$\overline{\Omega} = \cup_{k=1}^{K} \overline{\Omega_k^{bb}},$$

where each "building block" Ω_k^{bb} is assumed to be the image of a reference one-stage fin $\hat{\Omega}$. For reference, we assume that $\hat{\Omega}$ is composed of four squares $\overline{\hat{\Omega}} = \cup_{j=1}^{4} \overline{\hat{\Omega}_j}$.

The mapping φ_k between $\hat{\Omega}$ and Ω_k^{bb} will be assumed to be piecewise linear and continuous so that

$$\Omega_k^{bb} = \varphi_k[\hat{\Omega}]$$

and $\varphi_{k|\hat{\Omega}_j}$ is affine. The problem we want to approximate reads as follows: Find $u \in H^1(\Omega)$ such that

$$a(u,v) = f(v) \qquad \forall\, v \in H^1(\Omega), \tag{4.1}$$

where, as in (2.4),

$$a(u,v) = \sum_{i=0}^{K} k_i \int_{\Omega_i^m} \nabla u \cdot \nabla v \; dA + \mathrm{Bi} \int_{\partial\Omega \setminus \Gamma_{\mathrm{root}}} u\, v \; dS, \tag{4.2}$$

$$f(v) = \int_{\Gamma_{\mathrm{root}}} q\, v \; dS. \tag{4.3}$$

The reduced basis element method assumes that $\hat{\Omega}$ is provided with basis functions $\hat{\zeta}_1, \hat{\zeta}_2, \ldots, \hat{\zeta}_M$ which are supposed to be linearly independent, and that are mapped over each Ω_k^{bb} through φ_k. We thus introduce the space

$$Y_M^2 = \{ v_M \in L^2(\Omega) | \quad v_{M|\Omega_k} \circ \varphi_k \in \mathrm{span}\{\hat{\zeta}_1, \hat{\zeta}_2, \ldots, \hat{\zeta}_M\} \}. \tag{4.4}$$

Note again that Y_M^2 is not an acceptable discretization space for $H^1(\Omega)$. We now define X_M^2 for this purpose by gluing the functions of Y_M^2 across the interfaces $\gamma_{k,\ell}^{bb}$ between two adjacent stages

$$\overline{\gamma}_{k,\ell}^{bb} = \overline{\Omega_k^{bb}} \cap \overline{\Omega_\ell^{bb}}. \tag{4.5}$$

Again, we use Lagrange multipliers to match the functions across the interfaces between the stages:

$$X_M^2 = \left\{ v_M \in Y_M^2 | \quad \int_{\gamma_{k,\ell}^{bb}} (v_{M|\Omega_k} - v_{M|\Omega_\ell}) \psi \, ds = 0 \quad \forall \psi \in W_{k,\ell} \right\}, \tag{4.6}$$

where we here limit the choice of the Lagrange muliplier space to low order polynomials,

$$W_{k,\ell} = \mathbb{P}_n(\gamma_{k,\ell}^{bb}).$$

The discrete problem then reads: Find u_M^2 in X_M^2 such that

$$a^{\mathcal{N}}(u_M^2, v) = f^{\mathcal{N}}(v) \qquad \forall v \in X_M^2. \tag{4.7}$$

4.2. Numerical results. This second way of generating the discrete spaces, deduced from a definition of more tuned reference shapes, has been tested on two different geometries. The first geometry is the three-stage fin used previously (see Figures 1–3); while the second one is the four-stage fin depicted in Figure 6. The differences between these two applications are first, the number of stages, and second, the fact that the geometries of the four stages are different together with the conductivities.[1]

[1] Of course, in the equation setting, that these two characteristics are linked as a change of variable allows us to describe a change of geometry as a change of parameter, but since Ω_0^m is kept fixed, it is not exactly equivalent.

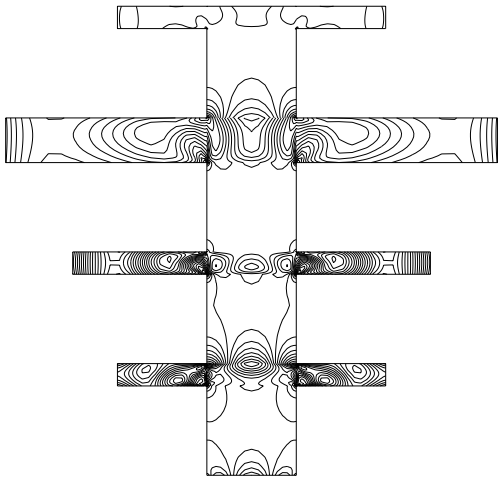

FIG. 6. *Geometry and error contours for the four-stage fin in the case of using $M = 16$ basis functions. Unlike the three-stage fin, each stage is different: The length and the thickness of the fins are different from stage to stage; the vertical distance between the various fins is here kept the same. Also, the center piece of the fin has a similar shape as the three-stage fin. The thermal conductivities for the subfins in the various stages are $k_1 = 0.2$, $k_2 = 0.4$, $k_3 = 0.6$, and $k_4 = 0.8$; as before, the conductivity for the center piece is $k_0 = 1$. We use the same basis functions for the four-stage fin as we use for the three-stage fin. We recall that all of these basis functions are based on various snapshots of a two-stage fin where the two stages are identical in geometric shape but with different values for k_1 and k_2.*

TABLE 3

	K=3 (three-stage fin)				K=4 (four-stage fin)			
M	n=1	n=2	n=3	n=4	n=1	n=2	n=3	n=4
6	0.0329	0.0403	0.1370	0.1820	0.0035	0.0783	0.5150	0.6320
8	0.0167	0.0189	0.0189	0.0212	0.0143	0.0149	0.0202	0.0350
10	0.0135	0.0114	0.0111	0.0159	0.0115	0.0128	0.0128	0.0232
12	0.0144	0.0094	0.0095	0.0112	0.0129	0.0094	0.0094	0.0115
14	0.0211	0.0055	0.0073	0.0068	0.0171	0.0078	0.0071	0.0079
16	0.0243	0.0039	0.0042	0.0045	0.0182	0.0034	0.0045	0.0052

We will now explain how the basis functions are determined. As before, we generate them on simple cases. We have here chosen to use a symmetric two-stage fin; the two stages are identical but with coefficients $k_1 \neq k_2$. The thickness of the fins may also vary. Each computed solution (i.e. each snapshot) is then split in two in order to define functions on the one-stage reference geometry. Each spectral evaluation thus gives rise to two basis functions; these do not need to be reflected since they *are* symmetric. As mentioned earlier, the matching between the stages is ensured through polynomial "gluing."

In Table 3, we present the errors between the "exact" solution $u^{\mathcal{N}}$ and the reduced basis element solution u_M^2 in the L^∞-norm obtained for various values of K, M, and n. The three-stage fin is the same as before, while the four-stage fin used in these experiments is depicted in Figure 6.

Note the impressive reduction of the size of the resulting system. For the three-stage fin, the same level of accuracy is obtained with method 2 with only eight or ten basis functions per stage, while method 1 requires 4×24 basis functions (using all three

snapshots). Compared to method 1, method 2 thus reduces the size of the algebraic system by a factor of 10. The additional work required to obtain this reduction is certainly worthwhile in applications where many evaluations have to be considered (e.g., in optimization processes or for time dependent problems). In addition, as will be seen in the next subsection, this strategy can be certified thanks to the a posteriori bounds.

4.3. A posteriori bounds. Assume that we are interested in the average temperature at the root of the fin:

$$s = \int_{\Gamma_{\text{root}}} u(t)dt.$$

The high accuracy provided by the solution $u^{\mathcal{N}}$ allows us to consider

$$s^{\mathcal{N}} = \int_{\Gamma_{\text{root}}} u^{\mathcal{N}}(t)dt = f^{\mathcal{N}}(u^{\mathcal{N}})$$

to be sufficiently accurate for our needs. Of course, implicitly, this output $s^{\mathcal{N}}$ is a function of the geometry of Ω, and thus of K and $\{\varphi_k\}_{k=1,\dots,K}$, as well as of the physical properties of the material $\{k_i\}_{i=0,\dots,K}$ and Bi; indeed, $u^{\mathcal{N}}$ itself depends on these parameters. The point now is that we do not want to compute $u^{\mathcal{N}}$; this may be the case if many geometries, with variable K, have to be considered.

The outcome of the reduced basis element method allows us instead to compute only u_M associated with a small number of basis elements M so that for each new geometry, the computation of u_M and thus of the corresponding output will be quite inexpensive. The main problem is now to be able to quantitatively certify the output. This is generally the aim of a posteriori error estimates, and in the frame of reduced basis functions, this has been developed in, e.g., [7, 9]. The main difference from the previous applications is in the fact that our approach is twice nonconforming—first, by the fact that the basis functions are stored on a geometry much simpler than the ones of interest (one stage versus many stages), and second, by the fact that the approximated solution is not globally in H^1.

In what follows, we are going to extend the a posteriori bound for output strategy that has been developed in a different context in [7].

The evaluation of bounds will follow three steps.

First step. Correction of the continuity at the interfaces. Our current solution u_M $(= u_M^2)$ suffers from being discontinuous at the interfaces. In order to correct this, we can simply solve a (local) Laplace problem on each square above the nonconforming interfaces with Dirichlet boundary conditions equal to the jump at this interface and zero on the opposite edge of the square, while zero Neumann conditions are set on the two last edges. The sum of u_M and the $K-1$ corresponding corrections will be denoted as $\tilde{u}_M$. It is an element of $\mathcal{X}^{\mathcal{N}}$, and it is easy to realize that the distance between $u^{\mathcal{N}}$ and $\tilde{u}_M$ can be bounded by a constant times the error between $u^{\mathcal{N}}$ and u_M. This follows easily from the stability of the lifting and the fact that the jump in u_M is, in the $H_{00}^{1/2}$-seminorm smaller than two times the difference between $u^{\mathcal{N}}$ and u_M. Note that $\tilde{u}_M$ is not the solution to some variational problem any more.

Second step. Derivation of a lower bound. We are going to compute, with a little extra work, a lower bound for $s^{\mathcal{N}}$ (of course without computing $u^{\mathcal{N}}$!). This is done by setting

$$s_M^- = 2f^{\mathcal{N}}(\tilde{u}_M) - a^{\mathcal{N}}(\tilde{u}_M, \tilde{u}_M). \tag{4.8}$$

The proof that this is a lower bound follows from the easy computation (recall that $q = 1$)

$$\begin{aligned} s^{\mathcal{N}} - s_M^- &= f^{\mathcal{N}}(u^{\mathcal{N}}) - 2f^{\mathcal{N}}(\tilde{u}_M) + a^{\mathcal{N}}(\tilde{u}_M, \tilde{u}_M) \\ &= a^{\mathcal{N}}(u^{\mathcal{N}}, u^{\mathcal{N}} - 2\tilde{u}_M) + a^{\mathcal{N}}(\tilde{u}_M, \tilde{u}_M) \\ &= a^{\mathcal{N}}(u^{\mathcal{N}} - \tilde{u}_M, u^{\mathcal{N}} - \tilde{u}_M) \\ &\geq 0. \end{aligned}$$

Note that this sequence of equalities also shows that the convergence of s_M^- toward $s^{\mathcal{N}}$ is quadratic in $\|u^{\mathcal{N}} - \tilde{u}_M\|_{H^1}$:

$$|s^{\mathcal{N}} - s_M^-| \leq c\,\|u^{\mathcal{N}} - u_M\|_*^2. \tag{4.9}$$

The previous derivation of a lower bound is quite simple and results from the fact that we are in the compliance case. For a general output, a dual problem needs to be introduced. However, the convergence rate and conclusion remain the same, but the derivation is more technical, though well known; see, e.g., [7, 9, 12, 13].

Last step. Derivation of an upper bound. There is here—as in other contexts—a little more work than for the previous step. The construction of the upper bound involves two ingredients. First, we design a partition of unity on Ω,

$$1 = \sum_{p=1}^{P} \chi_p, \quad \chi_p \geq 0,$$

of $\mathcal{C}^0(\Omega)$ functions so that the support of χ_p is composed typically of two, three, or four (spectral) elements. We can choose χ_p as being piecewise biaffine (i.e., elements of $\mathbb{P}_1$). Let ω_p stand for the support of χ_p that we assume to be comprised of three spectral elements. Let $\hat{\omega}$ be an L-shaped domain, the union of three squares $\hat{\omega}_i$, $i = 1, \ldots, 3$, with edge length equal to 2. By using the mapping φ_k it is an easy matter to define mappings denoted as ψ_p from $\hat{\omega}$ over ω_p, $p = 1, \ldots, P$. We consider now the bilinear form $\hat{a}$ defined as

$$\hat{a}(u, v) = \int_{\hat{\omega}} \nabla u \nabla v + \int_{\hat{\omega}} uv.$$

It is easy to check that there exist constants σ_p, $p = 1, \ldots, P$, such that

$$a^{\mathcal{N}}(v, v) \geq \sum_{p=1}^{P} \sigma_p \hat{a}^{\mathcal{N}}(v \circ \psi_p, v \circ \psi_p) \quad \forall v \in \mathcal{X}^{\mathcal{N}}. \tag{4.10}$$

Here, $\hat{a}^{\mathcal{N}}(\cdot, \cdot)$ refers to evaluating $\hat{a}(\cdot, \cdot)$ using Gauss–Lobatto–Legendre (GLL) quadrature. We refer to [9] and to the next subsection for a methodology for estimating the constants σ_p.

We are now in a position to define the local reconstructed errors; these will be piecewise polynomials defined over $\mathcal{X}^{\mathcal{N}}(\hat{\omega})$,

$$\mathcal{X}^{\mathcal{N}}(\hat{\omega}) = \{\, v \in H^1(\hat{\omega}),\, v_{|\hat{\omega}_i} \in \mathbb{P}_{\mathcal{N}}(\hat{\omega}_i),\, i = 1, \ldots, 3 \,\},$$

and defined by the following: Find $\hat{e}_p \in \mathcal{X}^{\mathcal{N}}(\hat{\omega})$ such that

$$\sigma_p \hat{a}(\hat{e}_p, v) = f^{\mathcal{N}}(\chi_p(v \circ (\psi_p)^{-1})) - a^{\mathcal{N}}(\tilde{u}_M, \chi_p(v \circ (\psi_p)^{-1})) \quad \forall v \in \mathcal{X}^{\mathcal{N}}(\hat{\omega}), \tag{4.11}$$

where we denote by the same function $v \circ (\psi_p)^{-1}$ the extension of $v \circ (\psi_p)^{-1}$ by zero in $\Omega \setminus \omega_p$.

Remark 1. In (4.11), the real problem should be

$$\sigma_p \hat{a}(\hat{e}_p, v) = f^{\mathcal{N}}(\mathcal{I}_N[\chi_p(v \circ (\psi_p)^{-1})]) - a^{\mathcal{N}}(\tilde{u}_M, \mathcal{I}_N[\chi_p(v \circ (\psi_p)^{-1})]) \quad \forall v \in \mathcal{X}^{\mathcal{N}}(\hat{\omega}),$$

where $\mathcal{I}_{\mathcal{N}}$ denotes the interpolation operator at the Gauss–Lobatto nodes inside each element Ω_k^e. However, we stick to (4.11) for the sake of simplicity, since the conclusion still holds.

Remark 2. There are P such spectral element problems to be solved. It has to be noticed first that these are independent and much smaller than the ones encountered for the solution of the global problem on the K-stage fin. Second, following the presentation of [7, 12], these problems can be solved efficiently and rapidly through a black box approach.

We now set

$$s_M^+ = 2f^{\mathcal{N}}(\tilde{u}_M) - a^{\mathcal{N}}(\tilde{u}_M, \tilde{u}_M) + \sum_{p=1}^{P} \sigma_p \hat{a}(\hat{e}_p, \hat{e}_p) \tag{4.12}$$

and prove that this is an upper bound to $s^{\mathcal{N}}$. Indeed, let us denote by e the true error $e = u^{\mathcal{N}} - \tilde{u}_M$. We then have

$$\begin{aligned} \sigma_p \hat{a}(\hat{e}_p, e \circ \psi_p) &= f^{\mathcal{N}}(\chi_p e) - a^{\mathcal{N}}(\tilde{u}_M, \chi_p e) \\ &= a^{\mathcal{N}}(u^{\mathcal{N}}, \chi_p e) - a^{\mathcal{N}}(\tilde{u}_M, \chi_p e) \\ &= a^{\mathcal{N}}(e, \chi_p e), \end{aligned}$$

which yields first

$$\begin{aligned} \sum_{p=1}^{P} \sigma_p \hat{a}(\hat{e}_p, e \circ \psi_p) &= \sum_{p=1}^{P} f^{\mathcal{N}}(\chi_p e) - \sum_{p=1}^{P} a^{\mathcal{N}}(\tilde{u}_M, \chi_p e) \\ &= f^{\mathcal{N}}(e) - a^{\mathcal{N}}(\tilde{u}_M, e) \end{aligned}$$

and second

$$\begin{aligned} \sigma_p \hat{a}(\hat{e}_p - e \circ \psi_p, \hat{e}_p - e \circ \psi_p) &= \sigma_p[\hat{a}(\hat{e}_p, \hat{e}_p) - 2\hat{a}(\hat{e}_p, e \circ \psi_p) + \hat{a}(e \circ \psi_p, e \circ \psi_p)] \\ &= \sigma_p \hat{a}(\hat{e}_p, \hat{e}_p) - a^{\mathcal{N}}(e, \chi_p e) - \sigma_p \hat{a}(\hat{e}_p, e \circ \psi_p) \\ &\quad + \sigma_p \hat{a}(e \circ \psi_p, e \circ \psi_p), \end{aligned}$$

which finally yields

$$\begin{aligned} \sum_{p=1}^{P} \sigma_p \hat{a}(\hat{e}_p, \hat{e}_p) &= \sum_{p=1}^{P} \sigma_p \hat{a}(\hat{e}_p - e \circ \psi_p, \hat{e}_p - e \circ \psi_p) + a^{\mathcal{N}}(e, e) + f^{\mathcal{N}}(e) \\ &\quad - a^{\mathcal{N}}(\tilde{u}_M, e) - \sum_{p=1}^{P} \sigma_p \hat{a}(e \circ \psi_p, e \circ \psi_p) \\ &\geq \sum_{p=1}^{P} \sigma_p \hat{a}(\hat{e}_p - e \circ \psi_p, \hat{e}_p - e \circ \psi_p) + f^{\mathcal{N}}(e) - a^{\mathcal{N}}(\tilde{u}_M, e) \\ &= \sum_{p=1}^{P} \sigma_p \hat{a}(\hat{e}_p - e \circ \psi_p, \hat{e}_p - e \circ \psi_p) + f^{\mathcal{N}}(u^{\mathcal{N}}) - 2f^{\mathcal{N}}(\tilde{u}_M) \\ &\quad + a^{\mathcal{N}}(\tilde{u}_M, \tilde{u}_M), \end{aligned}$$

where the inequality follows from (4.10). Inserting this inequality into the definition of s_N^+ yields

$$s_M^+ \geq f^{\mathcal{N}}(u^{\mathcal{N}}) + \sum_{p=1}^{P} \sigma_p \hat{a}(\hat{e}_p - e \circ \psi_p, \hat{e}_p - e \circ \psi_p) \geq s^{\mathcal{N}}. \tag{4.13}$$

Similar to previous (conforming) a posteriori analysis for reduced basis methods, it can also be proven that

$$|s^{\mathcal{N}} - s_M^+| \ \leq \ c \, \|u^{\mathcal{N}} - u_M\|_*^2. \tag{4.14}$$

We refer to a future reference for the actual proof of (4.14). In what follows, we illustrate the effectivity of the lower and upper bounds.

4.4. Numerical results. W now provide numerical evidence to support the theoretical results discussed above. Specifically, we compute the lower bound gap $\Delta_M^- = s^{\mathcal{N}} - s_M^-$ and the upper bound gap $\Delta_M^+ = s_M^+ - s^{\mathcal{N}}$ for the four-stage fin depicted in Figure 6.

The first step is to construct the conforming approximation $\tilde{u}_M$ from u_M. To this end, we extend the discontinuity at the interface between the various stages by solving the Laplace equation in the single spectral element right above each interface. The boundary conditions along the edges of this single element are as follows: on the lower edge, the discontinuity is imposed as nonhomogeneous Dirichlet boundary conditions; on the upper edge, homogeneous Dirichlet conditions are imposed. On the two vertical edges, we have tried two alternatives: (i) homogeneous Dirichlet boundary conditions, and (ii) homogeneous Neumann conditions (as suggested in the theoretical part).

Once the harmonic extensions of the discontinuities between the stages have been constructed, we can add these harmonic extensions to u_M in order to produce the conforming approximation $\tilde{u}_M$. Following (4.8) and (4.12), this approximation is then used to compute the lower and upper bounds.

The values for the constants σ_p needed in order to compute the upper bound in (4.12) are obtained in the following way. We first use the fact that the right-hand side of (4.10) can be bounded as

$$\sum_{p=1}^{P} \sigma_p \hat{a}^{\mathcal{N}}(v \circ \psi_p, v \circ \psi_p) \ \geq \ \sigma_{\min} \sum_{p=1}^{P} \hat{a}^{\mathcal{N}}(v \circ \psi_p, v \circ \psi_p),$$

where $\sigma_{\min}$ is a constant (e.g., the minimum over all σ_p). We then find $\sigma_{\min}$ as

$$\sigma_{\min} = \min_{v \in \mathcal{X}^{\mathcal{N}}} \frac{a^{\mathcal{N}}(v, v)}{\sum_{p=1}^{P} \hat{a}^{\mathcal{N}}(v \circ \psi_p, v \circ \psi_p)}$$

by performing a simple inverse Rayleigh quotient iteration. Finally, we set $\sigma_p = \sigma_{\min}$, $p = 1, \ldots, P$. Note that the above procedure is not optimal either from the computational point of view or from the choice $\sigma_p = \sigma_{\min}$ and can be improved. More precisely, the evaluation of $\sigma_{\min}$ can be done from precomputed local eigenfunctions (on a single stage) by using the modal synthesis approach; see [3]. The local eigenfunctions can further be rapidly computed from reduced basis eigenspaces as explained in [9].

In Table 4, we report the lower bound gap $\Delta_M^- = s^{\mathcal{N}} - s_M^-$ and the upper bound gap $\Delta_M^+ = s_M^+ - s^{\mathcal{N}}$, both divided by the output $s^{\mathcal{N}} = 1.948655$, as a function of the

TABLE 4
Lower and upper bound gaps.

M	$\Delta_M^- \,/\, s^{\mathcal{N}}$	$\Delta_M^+ \,/\, s^{\mathcal{N}}$
6	$1.41 \cdot 10^{-2}$ $(1.41 \cdot 10^{-2})$	$2.15 \cdot 10^{-1}$ $(2.15 \cdot 10^{-1})$
8	$1.81 \cdot 10^{-3}$ $(1.82 \cdot 10^{-3})$	$2.32 \cdot 10^{-2}$ $(2.34 \cdot 10^{-2})$
10	$1.34 \cdot 10^{-3}$ $(1.35 \cdot 10^{-3})$	$1.62 \cdot 10^{-2}$ $(1.64 \cdot 10^{-2})$
12	$7.95 \cdot 10^{-4}$ $(8.06 \cdot 10^{-4})$	$1.37 \cdot 10^{-2}$ $(1.39 \cdot 10^{-2})$
14	$4.40 \cdot 10^{-4}$ $(4.44 \cdot 10^{-4})$	$6.81 \cdot 10^{-3}$ $(6.88 \cdot 10^{-3})$
16	$2.14 \cdot 10^{-4}$ $(2.14 \cdot 10^{-4})$	$2.62 \cdot 10^{-3}$ $(2.62 \cdot 10^{-3})$

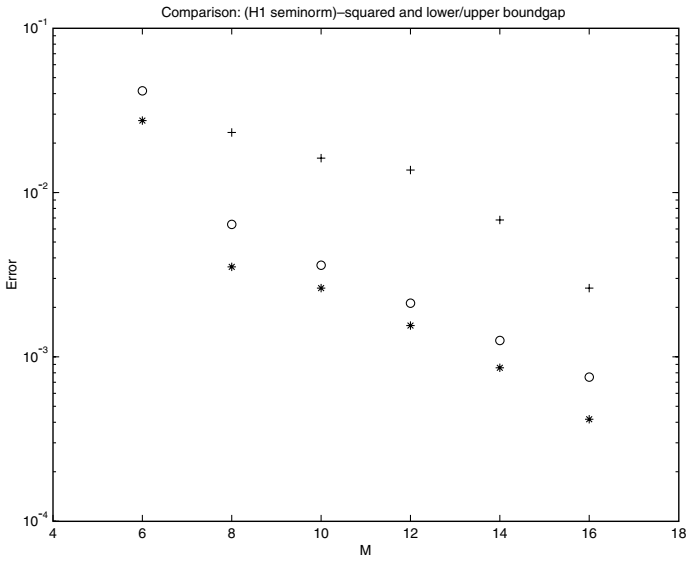

FIG. 7. *Convergence results for* Δ_M^- $(\star)$, Δ_M^+ $(+)$, *and* $\|u^{\mathcal{N}} - u_M\|_*^2$ $(\circ)$.

number of reduced basis functions M. First, we note that the sign of the bound gaps are correct, even for low values of M. Second, we report the bound gaps for the two different alternatives for boundary conditions when computing the harmonic extension. As expected, imposing homogeneous Neumann conditions along the vertical edges gives the lowest bound gaps for a fixed M. However, the difference between the two alternatives is very small, and the full Dirichlet case (the numerical results reported inside the parentheses) may be preferable due to a simpler implementation. We should remark that this conclusion is based only on this particular four-stage fin problem.

Next, we compare Δ_M^- and Δ_M^+ with $\|u^{\mathcal{N}} - u_M\|_*^2$. From Figure 7, we see that both the lower and upper bound gaps converge at least as fast as the square of the reduced-basis error in the H^1-seminorm, computed here as the broken norm over all the stages in the fin. The results are in accordance with (4.9) and (4.14).

5. Conclusions. We have presented a reduced basis element solution as an alternative to a "standard" spectral element solution for a particular application, namely, the numerical solution of a thermal fin problem. The numerical results indicate that it is possible to obtain solutions which are quite accurate using significantly fewer degrees-of-freedom than a more conventional approach. It is important, and actually

doable, to use bricks that are nonstandard. This allows us to obtain a significant reduction in the size of the discrete problem.

A point that has not been addressed in this paper is the possibility of combining offline/online computations to get a speed up factor when the approximation is required. This black box methodology, already developed in [7, 12], will be used in further developments.

The reduced basis element method is interesting as a potential method to solve complex problems where the global nature of the solution can be broken down into many local solutions with some similarity. The issue of a posteriori error estimation has also been addressed in this paper but has to be pushed forward in order to increase the efficiency of the predictions (see [13]). Indeed, this a posteriori analysis is as important as the design of good reference solutions. In summary, the reduced basis element methods have terrific speed up possibilities, but they need to be ascertained. The a posteriori tool is exactly what is required to discriminate between good solutions and unresolved ones.

The reduced basis element method may also be an interesting method for obtaining real time solutions to processes described by a set of partial differential equations; the extension to the time dependent case will be reported elsewhere, as will the application to nonlinear problems.

REFERENCES

[1] F. Ben Belgacem, *The mortar finite element method with Lagrange multipliers*, Numer. Math., 84 (1999), pp. 173–197.

[2] A. Berger, R. Scott, and G. Strang, *Approximate boundary conditions in the finite element method*, in Convegno di Analisi Numerica, INDAM, Rome, 1972, Sympos. Math. 10, Academic Press, London, 1972, pp. 295–313.

[3] I. Charpentier, F. De Vuyst, and Y. Maday, *Méthode de synthèse modale avec une décomposition de domaine par recouvrement*, C. R. Acad. Sci. Paris Sér. I Math., 322 (1996), pp. 881–888.

[4] C. Bernardi and Y. Maday, *Polynomial approximation of some singular functions*, Appl. Anal., 42 (1991), pp. 1–32.

[5] C. Bernardi, Y. Maday, and A. T. Patera, *A new nonconforming approach to domain decomposition: The mortar element method*, in Nonlinear Partial Differential Equations and Their Applications, College de France Seminar Vol. II, Pitman Res. Notes Math. Ser. 299, H. Brezis and J. L. Lions, eds., Longman Harlow, UK, 1994, pp. 13–51.

[6] J. P. Fink and W. C. Rheinboldt, *On the error behaviour of the reduced basis technique for nonlinear finite element approximations*, ZAMM Z. Angew. Math. Mech., 63 (1983), pp. 21–28.

[7] L. Machiels, Y. Maday, A. T. Patera, and D. V. Rovas, *A blackbox reduced-basis output bound method for shape optimization*, in Proceedings of the 12th International Conference on Domain Decompostion Methods, Chiba, Japan, 1999, T. Chan, T. Kako, H. Kawarada, and O. Pironneau, eds., DDM.org, 2001, pp. 429–436.

[8] Y. Maday and A. T. Patera, *Spectral element methods for the Navier-Stokes equations*, in State of the Art Surveys in Computational Mechanics, A. K. Noor, ed., ASME, New York, 1989, pp. 71–143.

[9] Y. Maday, A. T. Patera, and D. V. Rovas, *A blackbox reduced-basis output bound method for noncoercive linear problems*, in Nonlinear Partial Differential Equations and Their Applications, Collège de France Seminar, Vol. 14, Stud. Math. Appl. 31, North–Holland, Amsterdam, 2002, pp. 533–569.

[10] Y. Maday and E. M. Rønquist, *A reduced basis element method*, J. Sci. Comput., 17 (2002), pp. 447–459.

[11] A. K. Noor and J. M. Peters, *Reduced basis technique for nonlinear analysis of structures*, AIAA J., 18 (1980), pp. 455–462.

[12] C. Prud'homme, D. V. Rovas, K. Veroy, Y. Maday, A. T. Patera, and G. Turinici, *Reliable real-time solution of parametrized partial differential equations: Reduced-basis output bounds methods*, J. Fluids Engrg., 124 (2002), pp. 70–80.

[13] K. Veroy, D. V. Rovas, and A. T. Patera, *A posteriori error estimation for reduced-basis approximation of parametrized elliptic coercive partial differential equations: "Convex inverse" bound conditioners*, ESAIM Control Optim. Calc. Var., 8 (2002), pp. 1007–1028.